THE JOURNAL OF PHYSICAL CHEMISTRY A

Article

pubs.acs.org/JPCA

Fluorescence Products from Terrylenediimide with Singlet Oxygen: Red, Green, and Near-Infrared Emission

Hongmei Zhao,[†] Kunhui Liu,[‡] Di Song,[†] and Hongmei Su*[,†,‡]

[†]Beijing National Laboratory for Molecular Sciences (BNLMS), Institute of Chemistry, Chinese Academy of Sciences, Beijing 100190, P. R. China

[‡]College of Chemistry, Beijing Normal University, Beijing 100875, P. R.China

Supporting Information

ABSTRACT: The rich photo-oxidation pathways and products of terrylenediimide (TDI) with singlet oxygen ($^1O_2$) have been examined by powerful computational approaches. Potential energy profiles and product fluorescence properties are characterized. A variety of new products are unraveled and predicted to emit fluorescence at both visible and near-infrared ranges, which could open the possibility for interesting applications of using TDI as a fluorescence probe for the single-molecule detection of $^1O_2$ and designing multicolor photoconvertible fluorophores based on $^1O_2$ oxidation.

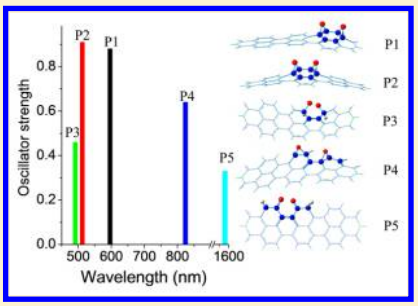

INTRODUCTION

Terrylenediimide (TDI) (Scheme 1) and its imide derivatives are superb polyaromatic hydrocarbon (PAH) colorants and have attracted intense research interests as functional dyes[1] widely used in various fields, such as photovoltaic devices,[2] nanoreporters,[3] biolabeling,[4] and light-harvesting systems.[5] They have been particularly successful for single-molecule investigations due to high photostability and fluorescent quantum yield.[6,7] Meanwhile, the photo-oxidation of TDI by single oxygen $^1O_2$ has been utilized to develop a sensitive and specific single-molecule method detecting $^1O_2$.[8] In the single-molecule imaging experiment of $^1O_2$, the TiO_2 film-coated slide glass was irradiated with UV light (365 nm) and underwent photocatalytic reactions to generate airborne $^1O_2$ molecules, which reacted with TDI, leading to the cycloaddition product, TDI diepoxide, with bright fluorescent spots emerging at 600 nm, ∼70 nm blue shift of the parent TDI. Assuming that a single TDI molecule is oxidized by a single $^1O_2$ molecule to form a TDI diepoxide, the number of $^1O_2$ could then be directly count using the signal of fluorescence spots of TDI diepoxide.

The TDI molecule is composed of three naphthalene units linked in the peri position (Scheme 1). In principal, the three naphthalene units are equally reactive when subject to the $^1O_2$ attack, and multiple fluorescent oxidation products are expected. Interestingly, the existence of other products has been indicated, where another product of TDI reacting with $^1O_2$ was observed with fluorescence at shorter wavelength (in the range of 510 to 570 nm), but the identity of this product remains unknown.[9] Several different green emissive photoproducts were recently reported for similar oxidizing reaction of TDI during photobleaching.[10] So far, knowledge about the photo-oxidation pathways and products of TDI by $^1O_2$ is rather limited, whereas this information is essential for the applications of TDI as a fluorescence sensor and probe.

Herein we address this issue from a theoretical perspective. By the use of density functional theory to unravel accessible reaction pathways and time-dependent DFT to optimize excited-state geometry as well as characterize product fluorescence properties, we show that multiple channels are expected for the oxidation of TDI by $^1O_2$, leading to a rich variety of fluorescence products, including three products fluorescing at visible range (red and green) and two other products fluorescing at near-infrared range. These findings provide illuminations for rational design of photoconvertible fluorophores based on $^1O_2$ oxidation reactions and also point to new methods of using TDI as a fluorescence probe for the detection of $^1O_2$, not only in the visible range but also in the near-infrared range.

THEORETICAL METHODS

The reaction pathways were located using the Gaussian 09[11] package with restricted B3LYP/6-31G* for all closed-shell species[12] and unrestricted (U)B3LYP/6-31G* calculations within the broken symmetry (BS) approach for open-shell diradical species.[13,14] The harmonic frequency analysis was performed to identify the stationary point as either local minima (reactant, products, and intermediates) or first-order saddle points (transition states) and to extract zero-point vibrational energy corrections. Connections of the transition

Special Issue: Piergiorgio Casavecchia and Antonio Lagana Festschrift

Received: December 30, 2015
Revised: February 5, 2016
Published: February 9, 2016

DOI: 10.1021/acs.jpca.5b12722
J. Phys. Chem. A 2016, 120, 5016−5022

Scheme 1. Molecular Structure of TDI (R = Alkyl or Phenyl) and the Oxygenated Adducts

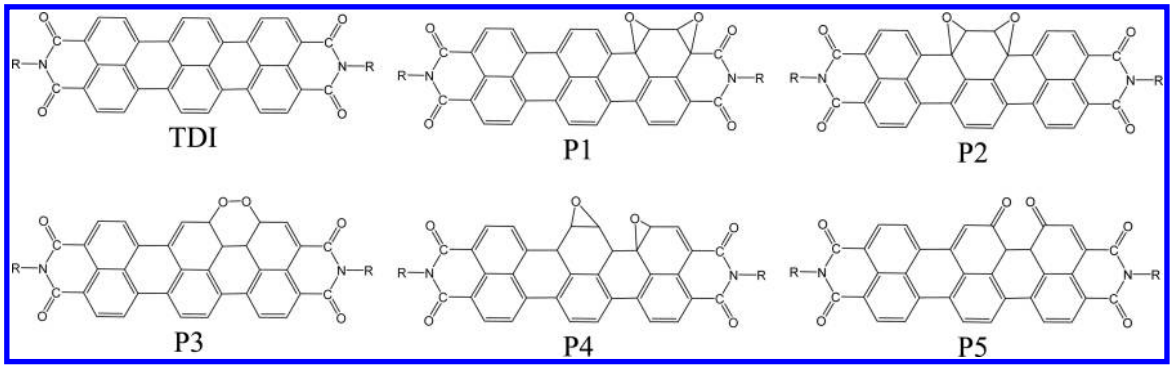

states between two local minima have been confirmed by intrinsic reaction coordinate (IRC) calculations at the same level. DFT within the broken symmetry (BS) is an appropriate quantum-chemical approach both in computational efficiency and in a balanced treatment of closed-shell and diradical species.[15] To further refine the energy and eliminate the spin contamination error, we used the approximate spin-projection (AP) method to calculate the spin-projected energies.[15,16] Density functional theory (using the B3LYP functional) has been shown to perform exceedingly well in studies involving biradicals,[17,18] which has also been successfully applied to study the reactions of $^1O_2$.[14] Other higher level methods such as a complete active space (CAS)[19,20] or multireference (MR) methods[21] cannot be applied for the current large system of TDI (with three naphthalene units) reacting with $^1O_2$ because of the inefficiency of computation with increasing size of system or number of active orbitals, especially to the potential energy surfaces, which include numerous possible reaction pathways and configurations for all resulting stationary points.

For all unraveled products, the peak wavelengths of the emission and absorption spectra were calculated using the Turbomol 6.0 program package.[22] To obtain the most accurate characteristics of fluorescence for molecules under investigation, it is necessary to use equilibrium geometries of the first excited singlet electronic state (S_1) because geometries of S_1 and S_0 states can be different.[23] Therefore, the TD-DFT methods with the B3LYP functional and the double-ζ quality basis sets of def-SVP[24] were applied to fully optimize the excited-state (S_1) equilibrium structures, from which the emission wavelengths and oscillator strength were computed. In all calculations, side chains irrelevant to the reaction, the alkyl and phenyl groups of TDI, are substituted by hydrogen atoms for the sake of computational efficiency.

RESULTS AND DISCUSSION

Product Formation Pathways. In this study, we investigated a large number of possible reaction pathways, including both the single attack and multiple attacks of $^1O_2$ molecules to TDI. The single attack of $^1O_2$ molecules to TDI occurs primarily and should dominate the product distributions. So we focus our examination on the reaction pathways involving a single reacting $^1O_2$ molecule. The calculated potential energy profiles are displayed in Figure 1. Basically, the reaction is initiated by the formation of either an endo- or exoperoxide, depending on the way of $^1O_2$ addition to TDI. Pathways 1 and 2 correspond to the endoperoxide reaction channels, whereas Pathway 3 represents the exoperoxide channels.

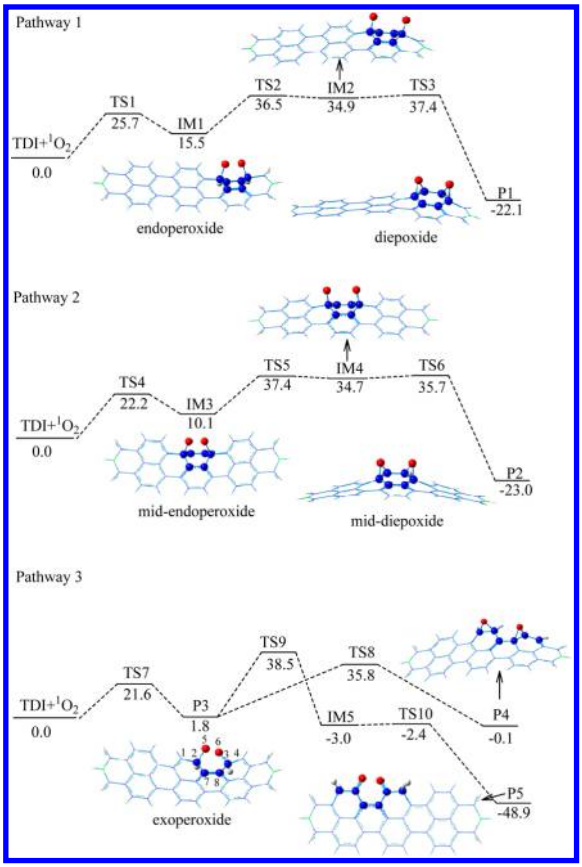

Figure 1. Potential energy profiles of the TDI reaction with $^1O_2$. All energies (in kcal mol^{-1}) given are relative to the reactants. Only the structures of key intermediates and products are displayed. The naphthalene units subject to $^1O_2$ addition are labeled with blue balls. Red balls represent oxygen atoms. See the Supporting Information for the detailed structures of each stationary point.

For Pathway 1, the attack of singlet oxygen to one of the two outer naphthalene rings in TDI via the Diels–Alder [4 + 2] cycloaddition leads to the first intermediate, TDI endoperoxide IM1, via concerted transition state TS1 overcoming a barrier of 25.7 kcal mol^{-1}. In agreement with previous studies on the reaction of singlet oxygen with benzene[25] and naphthalene,[14] only the single-step concerted mechanism with the symmetric transition-state structure to form endoperoxide is found for the [4 + 2] cycloaddition of $^1O_2$ to TDI. The endoperoxide IM1 is unstable (15.5 kcal mol^{-1} above the reactant) and will undergo successive reaction steps to form thermodynamically more stable products. So the simple O–O bond (1.476 Å) fission of

DOI: 10.1021/acs.jpca.5b12722
J. Phys. Chem. A 2016, 120, 5016–5022

endoperoxide occurs via TS2 with the O−O bond length of 2.278 Å (shown in Figure S1), leading to the second intermediate IM2. According to the Mulliken atomic spin density analysis, IM2 is of a diradical character, with spin densities mainly localized on the endoperoxide O1 and O2 atoms, and the O−O bond length is 2.967 Å, as shown in Figure 2 and Figure S1. The diradical feature makes IM2 highly

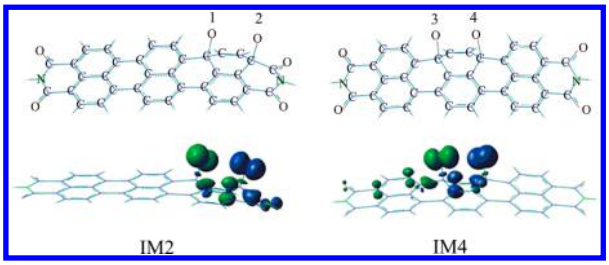

Figure 2. Calculated geometric structures (upper) and spin density distribution (lower) for the two diradical intermediates IM2 and IM4. The blue contour represents the spin up density, while the green contour represents the spin down density. The surface isovalue used is 0.005 au.

reactive and rearranges easily via ring-closure to the end product, diepoxide P1, as manifested by its low barrier of 2.5 kcal mol^{-1} (from IM2 to TS3). The diepoxide P1 lies 22.1 kcal mol^{-1} below the reactants, indicating that this product pathway is thermodynamically favorable. The rate-limiting barrier (25.7 kcal mol^{-1}) for P1 formation pathway is comparable and in line with those obtained for similar reactions of polyaromatic hydrocarbons with $^1O_2$,[25] while it is well recognized that polyaromatic hydrocarbons react readily with $^1O_2$. It is anticipated that the formation of diepoxide P1 could occur under the standard-temperature conditions. Indeed, this product has been observed and identified in the single-molecule $^1O_2$ imaging experiment.[8]

Analogous to Pathway 1, Pathway 2 occurs also through the [4 + 2] cycloaddition. Here $^1O_2$ is added to the central naphthalene ring of TDI, forming the midendoperoxide IM3 with a barrier of 22.2 kcal mol^{-1}. Subsequently, the homolytic rupture of the O−O bond (1.474 Å) of midendoperoxide IM3 forms the intermediate IM4. IM4 is also a diradical, featured by the localization of spin densities on the midendoperoxide O3 and O4 atoms (Figure 2) with the O−O bond length of 2.698 Å (Figure S1). Thus, the highly reactive intermediate IM4 is followed by a facile low barrier rearrangement to the stable end product, mid-diepoxide P2. The product P2 lies 23.0 kcal mol^{-1} below the reactants and is thermodynamically as stable as the product P1.

In competition with the endoperoxide Pathways 1 and 2, there exists also an exoperoxide Pathway 3. As shown in Figure 1, the addition of $^1O_2$ to the carbon atoms of two neighboring naphthalene units in TDI overcomes a barrier of 21.6 kcal mol^{-1}, leading to the exoperoxide P3. Unlike the endoperoxides in Pathways 1 and 2 that are unstable intermediates, the exoperoxide P3 formed in Pathway 3 is isoenergetic with the reactant (only 1.8 kcal mol^{-1} above the reactant) and can be regarded as a relatively stable primary product. This result explains the observation that a similar exoperoxide product was identified as the main photo-oxidation product of a single terrylene molecule by $^1O_2$ doped in the *p*-terphenyl crystal.[26]

All carbon atoms in TDI are in one plane and the π-conjugation is delocalized along the carbon skeleton of TDI. The addition of $^1O_2$ molecules to TDI will change the planar structure and the degree of π-conjugation. The structures of TS1 in pathway 1, TS4 in pathway 2, and TS7 in pathway 3 are shown in Figure S2. After $^1O_2$ addition, the two carbon atoms (C1, C2) of the naphthalene ring are pushed to the outside of the carbon skeleton plane for TS1 and TS4, whereas TS7 still maintains the planar carbon skeleton. For TS1 and TS4, the planar structure distortion brought by $^1O_2$ attack is larger than that for TS7. Therefore, the barrier height of TS7 in pathway 3 is the lowest. As for TS1 and TS4, although both distorted, the symmetry of TS4 is better than TS1, which might be the reason that the energy of TS4 is a bit lower than TS1.

Starting from the exoperoxide P3, two successive channels leading to thermodynamically more stable products could occur (Figure 1). One is the homolytic cleavage of the peroxidic bond and rearrangement to the diepoxide product. Unlike the case in endoperoxide, the O−O bond fission of the exoperoxide P3 takes place asymmetrically due to the naphthalene ring distortion, forming the asymmetrical diepoxide product P4 (O5 bonding with C1 and C2, O6 bonding with C3 and C8). Another successive channel occurs through two hydrogen-transfer steps (from C2 to C1 and from C3 to C4), leading to the more stable carbonyl compound P5, with a formation heat of 48.9 kcal mol^{-1}. The hydrogen transfer allows the transition of the carbon atoms (C2 and C3) from sp^3 hybridization to sp^2 characteristics, which makes the planar structure of the carbon skeleton recovered for P5. P5 exhibits significantly more stability than P3 and falls around the global minimum of the potential energy surface.

Overall, these thermodynamically favorable pathways of TDI with $^1O_2$ are anticipated to yield five stable products. In addition to the diepoxide P1 that has been experimentally identified,[8] four other new products are predicted, that is, mid-diepoxide P2, exoperoxide P3, asymmetrical diepoxide P4, and carbonyl product P5. Are these products fluorescent? We performed further calculations. The geometries of the electronically excited states were fully optimized without any constraints using TD-DFT method at the B3LYP/def-SVP level, and the fluorescence optical transition energies were calculated. The obtained peak fluorescence wavelength and the oscillator strength are listed in Table 1 and compared with experimental fluorescence spectra if available.

Table 1. Product Fluorescence Peak Wavelength (λ) and Oscillator Strengths (f) obtained at the TD-B3LYP/def-SVP Level, Compared with Experimental Values if Available

product	λ (nm)	f	experiment[8,9] (nm)
P1	596	0.88	~600
P2	512	0.91	~510−570[a]
P3	491	0.46	[b]
P4	824	0.64	[b]
P5	1590	0.33	[b]

[a]Exact value was not reported. [b]Not detected.

Red and Green Emissive Products. The diepoxide P1 was the fluorescent product identified in the single-molecule imaging experiment, where TDI was used as a probe to detect the airborne $^1O_2$ molecule diffused from the surface of TiO_2 nanoparticles.[8] After UV irradiation of the sample for 5 min, bright fluorescent spots of the products was observed to arise quickly. For the bright spots that emerged the fluorescence spectra exhibited a peak wavelength at ~600 nm, with a strong

DOI: 10.1021/acs.jpca.5b12722
J. Phys. Chem. A 2016, 120, 5016−5022

fluorescence intensity and ~70 nm blue shift relative to the parent TDI. This fluorescent product was assigned to TDI diepoxide[8] according to the calculated absorption wavelength at the TD-B3LYP/3-21G* level, which showed a blue-shift tendency of the fluorescence spectra due to the formation of the TDI diepoxide. Here this assignment can be further supported by the calculations (at the higher level of TD-B3LYP/def-SVP) for the emission wavelength of all relevant species, which can be compared directly with experimental observations. As shown in Table 1, the calculated emission wavelength of TDI diepoxide is 596 nm, with large oscillator strength of 0.88, indicating a strong fluorescence at 596 nm for this product. The calculated results are in excellent agreement with the experimentally observed bright fluorescence centered at ~600 nm, confirming the identification of the diepoxide P1 as one of the major fluorescent products from the reaction of TDI with $^1O_2$. Furthermore, the agreement with the experimental observation demonstrates that the current level of calculations can provide accurate theoretical predictions for fluorescence properties. The following predictions of new fluorescent products are based on this comparison for the known product diepoxide P1 first.

The second predicted major fluorescent product is the mid-diepoxide P2, generated from Pathway 2. Pathway 2 proceeds through similar steps to those of Pathway 1, except that $^1O_2$ is added to the central naphthalene ring of TDI. The overall barrier of the mid-diepoxide P2 formation along Pathway 2 is equivalent to those of the diepoxide P1 along Pathway 1. Therefore, it is anticipated that the mid-diepoxide P2 is also one of the major products and should be detected in the experiment, as has been done for the diepoxide P1.[8] According to our TD-DFT calculations (Table 1), the emission wavelength of mid-diepoxide P2 is 512 nm, with a oscillator strength of 0.91, which is even larger than that of the diepoxide P1. So it is predicted that the mid-diepoxide P2 is also brightly fluorescent with the peak wavelength at 512 nm.

This product fluoresces at much shorter wavelength (~160 nm blue-shifted) relative to the parent TDI, shifting out of the resonance when the fluorescence was probed upon 532 nm laser excitation and thus was not detected,[8] but with shorter wavelength laser excitation at 488 nm, a fluorescent product of TDI reacting with $^1O_2$ was observed, with the emission emerging in the range of 510 to 570 nm.[9] The exact peak wavelength of the fluorescence was not given, and it was proposed that the new product was probably ascribed to the multiple attacks of $^1O_2$ molecules to TDI diepoxide.

According to our calculations, the yield of the mid-diepoxide P2 should be as important as that of the diepoxide P1, produced together with P1 as one of the major single attack products of TDI with $^1O_2$. In addition, P2 is predicted to brightly emit fluorescence at 512 nm. So the mid-diepoxide P2 is also a strong candidate to account for the unidentified product with fluorescence at shorter wavelength (510 to 570 nm) upon 488 nm excitation. Further experiments are highly desirable to examine in detail the fluorescence spectra for this predicted new product, the mid-diepoxide P2. Promisingly, we anticipate strong fluorescence to emerge at ~512 nm and can be detected in future experiments. Here the fluorescence intensity is predicted mainly by the calculated oscillator strength. The real fluorescence intensity (the quantum yield) should also be affected by the kinetic competition between the radiative deactivation channel and nonradiative deactivation channels, which is out of the scope of current theoretical studies; however, the bright fluorescence feature of the diepoxide product P1 has been demonstrated in experiments[8] and our predictions for P1 coincide with experiments. Presumably, the analogous product P2 (mid-diepoxide) behaves similarly given that its fluorescence oscillator strength is even larger. We also calculated the vertical S_0-S_1 transition energies and obtained the maximum absorption wavelengths (Table S1), which is 456 nm for P2. This provides a basis for choosing an appropriate excitation wavelength in future fluorescence detection experiments.

Possibilities of the multiple attacks of $^1O_2$ to diepoxide P1 have also been explored (see Supporting Information). Among the possible multiple attack products (Table S2), four products P6 (547 nm), P7 (553 nm), P13 (509 nm), and P14 (506 nm), are expected to be fluorescent around the range of 510 to 570 nm. We calculated the potential energy profiles for the multiple attack reactions forming these four products (Figure 3). P6 and

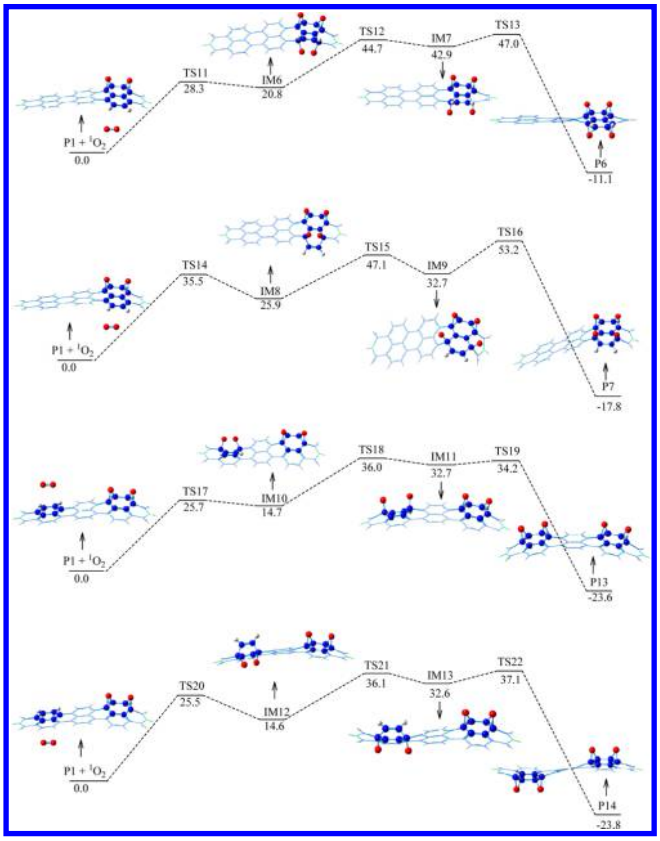

Figure 3. Potential energy profiles for the formation of $^1O_2$ multiple attack product P6, P7, P13, and P14 resulted from the second singlet oxygen being added to the primary product diepoxide P1. All energies (in kcal mol^{-1}) given are relative to the reactants of P1 with $^1O_2$.

P7 are formed when the second singlet oxygen is added to the same naphthalene unit of the diepoxide P1, but the reaction pathways for P6 or P7 encounter overall barriers of 47.0 or 53.2 kcal mol^{-1}, respectively (Figure 3), much higher than those of the single attack pathways (Figure 1), and thus should be more difficult to occur. This is understandable considering the extra structural distortion brought by the addition of the second singlet oxygen to the same naphthalene unit, whereas for P13 and P14, the products formed when the second singlet oxygen is added to another naphthalene unit of the diepoxide P1 (Figure 3), the reaction pathways only involve overall barriers

DOI: 10.1021/acs.jpca.5b12722
J. Phys. Chem. A 2016, 120, 5016−5022

of 36.0 and 37.1 kcal mol^{-1}, respectively, equivalent to those of the single attack pathways (Figure 1). Therefore, the multiple $^1O_2$ attack products P13 and P14 may also contribute to the observed fluorescence at shorter wavelength range of 510 to 570 nm, supporting the previous postulation.[9]

Although energetically accessible, the formation of the multiple attack products P13 and P14 should lag behind those of the single attack products kinetically and thus happen only after prolonged irradiation. Hopefully, for the possible products contributing to the fluorescence range of 510 to 570 nm, the real time formation of the single attack product P2 can be discerned from the multiple attack products P13 and P14, by tracking the time course of on−off fluorescence events in future single-molecule experiments.

In parallel to the formation of the two diepoxide products P1 and P2, the exoperoxide P3 is formed as a primary product, isoenergetic with the reactant (Pathway 3 in Figure 1). The barrier involved is 21.6 kcal mol^{-1}, which is also energetically accessible for standard-temperature conditions. The calculated fluorescence peak wavelength for the exoperoxide P3 is 491 nm, with oscillator strength of 0.46. So it is anticipated that the exoperoxide P3 could be identified by probing fluorescence spectra peaked at 491 nm upon appropriate shorter wavelength excitation. The predicted absorption maximum for P3 is at 452 nm (Table S1).

Here several blue-shifted fluorescent oxidation products are predicted for the reaction of TDI with singlet oxygen $^1O_2$, with fluorescence at 596, 512, and 491 nm for P1, P2, and P3, respectively. These results can find analogue in a recent single-molecule study,[10] where several different green emissive photoproducts due to photobleaching of TDI by ground-state oxygen were observed, emitting fluorescence at 600, 575, and 527 nm in the polymer film, respectively. It was also pointed out that the formation mechanisms and chemical structures of these ground-state oxygen oxidation products should be similar to those due to singlet oxygen, although with less conversion efficiency for ground-state oxygen oxidation (∼5%).[10] Such analogous results corroborate our theoretical predictions. Interestingly, both of our results and this recent experimental study demonstrate that the oxidation of TDI by either ground-state oxygen or singlet oxygen can both reduce molecular conjugation degree and thus lead to green emissive photoproducts, providing new photoconvertible fluorophores with green emission similar to the commonly used dyes of perylene diimide (PDI) or perylene monoimide (PMI).[10]

The new pathways and product fluorescence properties predicted here for TDI reacting with singlet oxygen can also provide hints to understand photobleaching behavior of rylene dyes by ambient ground-state oxygen. For example, in the TDI photobleaching experiment[10] intriguing behavior was also observed for the significantly blue-shifted green photoproducts, with significant variation in the extent of the blue shift over time or the capability to switch back to the original TDI emission spectrum. It was speculated that some TDI photoproducts with oxygen adducts in the bay area may be related to these phenomena.[10] Our results confirm this hypothesis. According to the calculated potential energy profiles (Figure 1), Pathway 3 forming exoperoxide P3 corresponds to the oxygen addition in the bay area of TDI. Indeed, P3 may have chances to undergo reversible reaction due to its lower formation heat and thermal stability among the three blue-shifted oxidation products (P1, P2, and P3). Hence, the reversible character for the exoperoxide P3 is expected, which can cause large spectral fluctuations due to switch back to the original TDI emission spectrum.[10]

Near-Infrared Emissive Products. On the contrary, as a relatively stable primary product, the exoperoxide P3 is subject to continuous laser irradiation, from which extra photon energies can be absorbed to surmount subsequent high barriers of Pathway 3 (Figure 1). So the successive formation of thermodynamically more stable products of the asymmetrical diepoxide P4 and the carbonyl product P5 can still occur. The calculated fluorescence wavelength for P4 is 824 nm with oscillator strength of 0.64 and that for P5 is 1590 nm with oscillator strength of 0.33, both lying in the near-infrared region with sufficiently strong fluorescence oscillator strength. This prediction may point to interesting applications of using TDI as a near-infrared (NIR) fluorescence probe for $^1O_2$, by monitoring the NIR fluorescence from the products of P4 and P5. It has been essential to develop NIR fluorescent probe for its importance in understanding the biological functions of $^1O_2$ and $^1O_2$-related photodynamic therapy.[27] Compared with the products fluorescing at visible, the NIR fluorescent products P4 and P5 may have several advantages serving as fluorophores, including the improved penetration, minimized tissue damage, and avoided influence of autofluorescence of NIR light in biological systems. For these reasons, the current findings of NIR fluorescent products P4 and P5 could render TDI potentially attractive NIR fluorescent probes for detecting $^1O_2$. The appropriate wavelength for exciting the NIR fluorescence can be chosen based on the calculated maximum absorption (Table S1), which is 710 and 902 nm for P4 and P5 respectively. It should be noted that although NIR fluorescent TDI oxidation product may be beneficial for in vivo observation, TDI itself is water-insoluble and cannot be directly applied to biological system, but promising strategies have been developed to improve solubility of such type of rylene dyes.[28]

CONCLUSIONS

Our calculations have predicted five products from single $^1O_2$ attack to TDI that are all fluorescent, including the known product diepoxide P1 and four other new products of mid-diepoxide P2, exoperoxide P3, asymmetrical diepoxide P4, and carbonyl product P5. For the first major product diepoxide P1, excellent agreement has been obtained between the calculated fluorescence wavelength of 596 nm and the experimental observation of 600 nm, demonstrating the accuracy of current level of calculations and providing rationale for the spectral identification in the single-molecule imaging experiment using TDI as a $^1O_2$ probe.[8] The second predicted major fluorescent product is the mid-diepoxide P2, with a large fluorescence oscillator strength at 512 nm. Although previously unidentified, this single attack major product P2, due to its product yield as important as that of P1, is very likely to contribute to the observed fluorescence at shorter wavelength (510 to 570 nm) upon 488 nm excitation, in addition to the previously postulated multiple attack products.[9]

For the other three single attack products that was previously unraveled, considerable fluorescence intensities are also expected, which are emitting at 491 nm for the exoperoxide P3, 824 nm for the asymmetrical diepoxide P4, and 1590 nm for the carbonyl product P5, respectively. The latter two products are probably suitable for developing NIR fluorescence $^1O_2$ probe, which requires further experimental studies to ascertain their fluorescence intensity and potential applications

DOI: 10.1021/acs.jpca.5b12722
J. Phys. Chem. A 2016, 120, 5016−5022

in living cells and tissues. Importantly, it shows here that the oxidation of TDI by singlet oxygen can modify molecular conjugation degree and thus lead to multicolor emissive photoproducts, covering fluorophore spectral range from red to green and NIR. The predictions of green emissive photoproducts for $^1O_2$ oxidizing TDI (512 and 491 nm) here can find analog in a recent single-molecule study on the photobleaching of TDI by ground-state oxygen,[10] and it appears that the ground-state oxygen oxidation products are similar to those due to singlet oxygen.[10] Further experiments on $^1O_2$ oxidizing TDI are certainly desirable to prove this scenario.

Altogether, the present findings provide mechanistic insights into understanding the rich photo-oxidation pathways and products of TDI by $^1O_2$, along with detailed spectral data (including both emission and absorption) that is valuable for assist deciphering the complex single-molecule fluorescence spectra. Such knowledge is essential for the application of TDI as a fluorescence sensor and opens the possibility for interesting new applications. The predicted new product pathways can also stimulate rational design of photoconvertible fluorophores based on TDI reaction with singlet oxygen. Hopefully, the current theoretical work will arouse the experimental interests, and further experiments could be performed to watch the reaction of TDI with $^1O_2$ at the level of single-molecule, from which the product distributions and reaction kinetics can be obtained.

■ ASSOCIATED CONTENT

Supporting Information

The Supporting Information is available free of charge on the ACS Publications website at DOI: 10.1021/acs.jpca.5b12722.

Optimized structures for reactants, intermediates, transition states, and products along potential energy profiles, the calculated product absorption wavelength and oscillator strengths, as well as the calculated fluorescence peak wavelength and oscillator strengths for the possible secondary products resulting from the multiple attack of $^1O_2$ to TDI. (PDF)

■ AUTHOR INFORMATION

Corresponding Author

*E-mail: hongmei@iccas.ac.cn. Tel: +86-10-62562837.

Notes

The authors declare no competing financial interest.

■ ACKNOWLEDGMENTS

This work was financially supported by the National Natural Science Foundation of China (Grants 21203206, 91441108, 21333012, and 21425313), National Basic Research Program of China (Grant 2013CB834602), and the Strategic Priority Research Program of the Chinese Academy of Sciences (Grant XDB12020200). We thank Prof. Andong Xia for helpful discussions. The calculations were supported by the Supercomputing Center, Computer Network Information Center of Chinese Academy of Sciences.

■ REFERENCES

(1) Weil, T.; Vosch, T.; Hofkens, J.; Peneva, K.; Müllen, K. The Rylene Colorant Family—Tailored Nanoemitters for Photonics Research and Applications. *Angew. Chem., Int. Ed.* **2010**, *49*, 9068−9093.

(2) Gorenflot, J.; Sperlich, A.; Baumann, A.; Rauh, D.; Vasilev, A.; Li, C.; Baumgarten, M.; Deibel, C.; Dyakonov, V. Detailed Study of N,N′-(diisopropylphenyl)-terrylene-3,4:11,12-bis(dicarboximide) as Electron Acceptor for Solar Cells Application. *Synth. Met.* **2012**, *161*, 2669−2676.

(3) Zürner, A.; Kirstein, J.; Döblinger, M.; Bräuchle, C.; Bein, T. Visualizing Single-Molecule Diffusion in Mesoporous Materials. *Nature* **2007**, *450*, 705−708.

(4) Schlichting, P.; Duchscherer, B.; Seisenberger, G.; Basché, T.; Bräuchle, T.; Müllen, K. A Bichromophore Based on Perylene and Terrylene for Energy Transfer Studies at the Single-Molecule Level. *Chem. - Eur. J.* **1999**, *5*, 2388−2395.

(5) Kim, H. N.; Puhl, L.; Nolde, F.; Li, C.; Chen, L.; Basché, T.; Müllen, K. Energy Transfer at the Single-Molecule Level: Synthesis of a Donor−Acceptor Dyad from Perylene and Terrylene Diimides. *Chem. - Eur. J.* **2013**, *19*, 9160−9166.

(6) Kukura, P.; Celebrano, M.; Renn, A.; Sandoghdar, V. Single-Molecule Sensitivity in Optical Absorption at Room Temperature. *J. Phys. Chem. Lett.* **2010**, *1*, 3323−3327.

(7) Feil, F.; Cauda, V.; Bein, T.; Bräuchle, C. Direct Visualization of Dye and Oligonucleotide Diffusion in Silica Filaments with Collinear Mesopores. *Nano Lett.* **2012**, *12*, 1354−1361.

(8) Naito, K.; Tachikawa, T.; Cui, S.-C.; Sugimoto, A.; Fujitsuka, M.; Majima, T. Single-Molecule Detection of Airborne Singlet Oxygen. *J. Am. Chem. Soc.* **2006**, *128*, 16430−16431.

(9) Naito, K.; Tachikawa, T.; Fujitsuka, M.; Majima, T. Real-Time Single-Molecule Imaging of the Spatial and Temporal Distribution of Reactive Oxygen Species with Fluorescent Probes: Applications to TiO2 Photocatalysts. *J. Phys. Chem. C* **2008**, *112*, 1048−1059.

(10) Liao, Z.; Hooley, E. N.; Chen, L.; Stappert, S.; Müllen, K.; Vosch, T. Green Emitting Photoproducts from Terrylene Diimide after Red Illumination. *J. Am. Chem. Soc.* **2013**, *135*, 19180−19185.

(11) Frisch, M. J.; et al. *Gaussian 09*, revision B.01; Gaussian, Inc.: Wallingford, CT, 2009.

(12) Becke, A. D. Density-Functional Thermochemistry. III. The Role of Exact Exchange. *J. Chem. Phys.* **1993**, *98*, 5648−5652.

(13) Kraka, E.; Cremer, D. The *para*-didehydropyridine, *para*-didehydropyridinium, and Related Biradicals—a Contribution to the Chemistry of Enediyne Antitumor Drugs. *J. Comput. Chem.* **2001**, *22*, 216−229.

(14) Reddy, A. R.; Bendikov, M. Diels−Alder Reaction of Acenes with Singlet and Triplet Oxygen − Theoretical Study of Two-State Reactivity. *Chem. Commun.* **2006**, 1179−1181.

(15) Goldstein, E.; Beno, B.; Houk, K. N. Density Functional Theory Prediction of the Relative Energies and Isotope Effects for the Concerted and Stepwise Mechanisms of the Diels−Alder Reaction of Butadiene and Ethylene. *J. Am. Chem. Soc.* **1996**, *118*, 6036−6043.

(16) Yamaguchi, K.; Jensen, F.; Dorigo, A.; Houk, K. N. A Spin Correction Procedure for Unrestricted Hartree-Fock and Møller-Plesset Wavefunctions for Singlet Diradicals and Polyradicals. *Chem. Phys. Lett.* **1988**, *149*, 537−542.

(17) Landis, C. R.; Morales, C. M.; Stahl, S. S. Insights into the Spin-Forbidden Reaction between L2Pd0 and Molecular Oxygen. *J. Am. Chem. Soc.* **2004**, *126*, 16302−16303.

(18) Chen, J. S.; Houk, K. N.; Foote, C. S. Theoretical Study of the Concerted and Stepwise Mechanisms of Triazolinedione Diels−Alder Reactions. *J. Am. Chem. Soc.* **1998**, *120*, 12303−12309.

(19) Roos, B. O.; Taylor, P. R.; Siegbahn, P. E. M. A Complete Active Space SCF Method (CASSCF) Using a Density Matrix Formulated Super-CI Approach. *Chem. Phys.* **1980**, *48*, 157−173.

(20) Andersson, K.; Malmqvist, P. Å.; Roos, B. O.; Sadlej, A. J.; Wolinski, K. Second-Order Perturbation Theory with a CASSCF Reference Function. *J. Phys. Chem.* **1990**, *94*, 5483−5488.

(21) Hirao, K. Multireference Møller—Plesset Method. *Chem. Phys. Lett.* **1992**, *190*, 374−380.

(22) Ahlrichs, R.; Baer, M.; Haeser, M.; Horn, H.; Koelmel, C. Electronic Structure Calculations on Workstation Computers: The Program System Turbomole. *Chem. Phys. Lett.* **1989**, *162*, 165−169.

DOI: 10.1021/acs.jpca.5b12722
J. Phys. Chem. A 2016, 120, 5016−5022

(23) Vyas, S.; Hadad, Ch.M.; Modarelli, D. A. A Computational Study of the Ground and Excited State Structure and Absorption Spectra of Free-Base N-Confused Porphine and Free-Base N-Confused Tetraphenylporphyrin. *J. Phys. Chem. A* **2008**, *112*, 6533−6549.
(24) Schäfer, A.; Horn, H.; Ahlrichs, R. Fully Optimized Contracted Gaussian Basis Sets for Atoms Li to Kr. *J. Chem. Phys.* **1992**, *97*, 2571−2577.
(25) Leach, A. G.; Houk, K. N. Diels−Alder and Ene Reactions of Singlet Oxygen, Nitroso Compounds and Triazolinediones: Transition States and Mechanisms from Contemporary Theory. *Chem. Commun.* **2002**, 1243−1255.
(26) Christ, T.; Kulzer, F.; Bordat, P.; Basché, T. Watching the Photo-Oxidation of a Single Aromatic Hydrocarbon Molecule. *Angew. Chem., Int. Ed.* **2001**, *40*, 4192−4195.
(27) Ogilby, P. R. Singlet Oxygen: There is Indeed Something New under the Sun. *Chem. Soc. Rev.* **2010**, *39*, 3181−3209.
(28) Yang, S. K.; Zimmerman, S. C. Polyglycerol-Dendronized Perylenediimides as Stable, Water-Soluble Fluorophores. *Adv. Funct. Mater.* **2012**, *22*, 3023−3028.

DOI: 10.1021/acs.jpca.5b12722
J. Phys. Chem. A 2016, 120, 5016−5022